

XMM-Newton Detection of Hot Gas in the Eskimo Nebula: Shocked Stellar Wind or Collimated Outflows? [★]

M. A. Guerrero¹, Y.-H. Chu², R. A. Gruendl², and M. Meixner³

¹ Instituto de Astrofísica de Andalucía, CSIC, Apartado Correos 3004, E-18080, Granada, Spain
e-mail: mar@iaa.es

² Astronomy Department, University of Illinois, 1002 W. Green Street, Urbana, IL 61801, USA
e-mail: chu@astro.uiuc.edu, gruendl@astro.uiuc.edu

³ Space Telescope Science Institute, 3700 San Martin Drive, Baltimore, MD 21218, USA
e-mail: meixner@stsci.edu

Received November 2004 / Accepted later 2004

Abstract. The Eskimo Nebula (NGC 2392) is a double-shell planetary nebula (PN) known for the exceptionally large expansion velocity of its inner shell, $\sim 90 \text{ km s}^{-1}$, and the existence of a fast bipolar outflow with a line-of-sight expansion velocity approaching 200 km s^{-1} . We have obtained *XMM-Newton* observations of the Eskimo and detected diffuse X-ray emission within its inner shell. The X-ray spectra suggest thin plasma emission with a temperature of $\sim 2 \times 10^6 \text{ K}$ and an X-ray luminosity of $L_X = (2.6 \pm 1.0) \times 10^{31} (d/1150 \text{ pc})^2 \text{ ergs s}^{-1}$, where d is the distance in parsecs. The diffuse X-ray emission shows noticeably different spatial distributions between the 0.2–0.65 keV and 0.65–2.0 keV bands. High-resolution X-ray images of the Eskimo are needed to determine whether its diffuse X-ray emission originates from shocked fast wind or bipolar outflows.

Key words. ISM: planetary nebulae: general – ISM: planetary nebulae: individual: NGC 2392 – stars: winds, outflows

1. Introduction

Planetary nebulae (PNe) consist of the stellar material ejected by low- and intermediate-mass stars ($1\text{--}8 M_{\odot}$) at the end of the asymptotic giant branch (AGB) phase. As such a star evolves off the AGB, the copious mass-loss strips off the stellar envelope and exposes the hot stellar core. A PN emerges when the stellar UV radiation ionizes the ejected stellar material, causing it to emit in the optical.

PNe are expected to be diffuse X-ray sources. The central stars of PNe possess fast stellar winds with terminal velocities of $1000\text{--}4000 \text{ km s}^{-1}$ (Cerruti-Sola & Perinotto, 1985), while fast collimated outflows with velocities up to 1000 km s^{-1} are also observed in PNe and proto-PNe, e.g., MyCn 18 and Hen 3-1475 (Bobrowsky et al., 1995; Riera et al., 1995; O’Connor et al., 2000). The interactions of the fast stellar wind and/or collimated outflows with nebular material produce shocked gas that is hot enough to emit in X-rays.

In the interacting-stellar-winds model of PNe (Kwok, Purton, & Fitzgerald, 1978), the fast wind emanating from the central star sweeps up the slow AGB wind to form a sharp nebular shell. The interior structure of a PN would be similar to that of a wind-blown bubble (e.g., Weaver et al.,

1977). The central cavity of a PN is expected to be filled with shocked fast wind at $10^7\text{--}10^8 \text{ K}$, but this hot gas is too tenuous to produce appreciable X-ray emission. Dynamic or evaporative mixing of cool nebular material into the hot gas at their interface produces optimal conditions for soft X-ray emission, which will show a limb-brightened morphology within the nebular shell, as observed in NGC 6543 (Chu et al., 2001).

Fast collimated outflows or jets may also produce hot X-ray-emitting gas. When outflows with velocities $\geq 300 \text{ km s}^{-1}$ initially impinge on the AGB wind, bow shocks and X-ray emission can be produced (e.g., Hen 3-1475, Sahai et al., 2003). The prolonged action of collimated outflows may bore through the AGB wind and form extended cavities filled by shocked hot gas that emits X-rays (e.g., Mz 3, Kastner et al., 2003).

Diffuse X-ray emission from hot gas in PNe was hinted by *ROSAT* observations (Guerrero, Chu, & Gruendl, 2000), but was unambiguously resolved only by *Chandra* and *XMM-Newton* observations. Besides the aforementioned Hen 3-1475, Mz 3, and NGC 6543, diffuse X-ray emission has been reported in only 4 other PNe: A 30, BD+30°3639, NGC 7009, and NGC 7027 (Chu, Chang, & Conway, 1997; Guerrero, Gruendl, & Chu, 2002; Kastner et al., 2000; Kastner, Vrtilik, & Soker, 2001). It is imperative to detect diffuse X-ray emission from a large number of PNe to investigate

Send offprint requests to: M. A. Guerrero

[★] Based on observations obtained with *XMM-Newton*, an ESA science mission with instruments and contributions directly funded by ESA Member States and NASA.

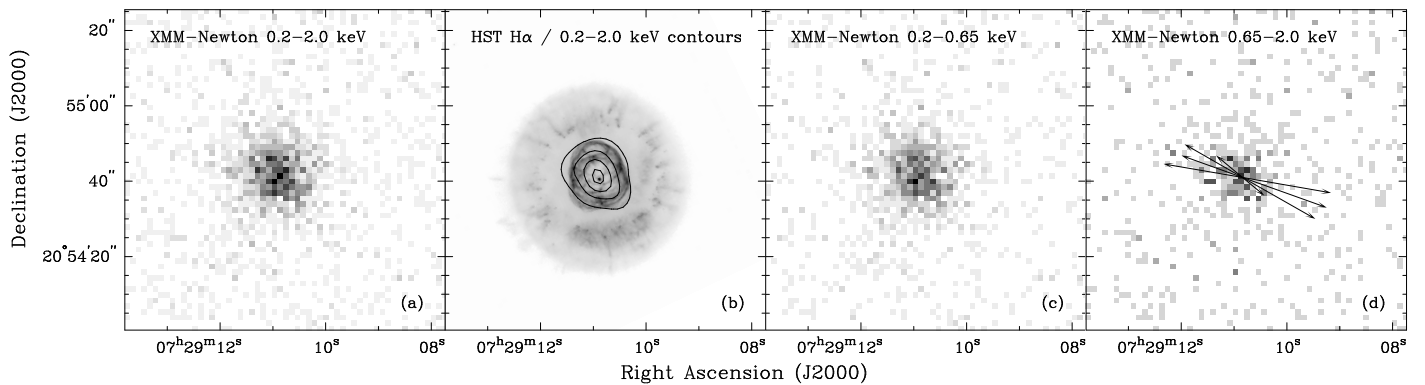


Fig. 1. *XMM-Newton* and *HST* $H\alpha$ images of the Eskimo Nebula. Panel (a) displays the *XMM-Newton* EPIC raw image in the 0.2–2.0 keV band with pixel size $1''.5$. Panel (b) shows the *HST* $H\alpha$ image overplotted by the 25%, 50%, 75%, and 95% X-ray contours extracted from the adaptively smoothed 0.2–2.0 keV band image described in the text. Contours at fainter levels are not plotted, as they show mainly the extended wings of *XMM-Newton*'s PSF and the smear caused by the adaptive smoothing. Panels (c) and (d) display *XMM-Newton* EPIC raw images in the 0.2–0.65 and 0.65–2.0 keV energy bands, respectively. The pixel size in these images is $1''.5$. The arrows in panel (d) mark the location of the fast collimated outflow as derived from high-dispersion echelle spectroscopy (Giesekeing, Becker, & Solf, 1985, Maestro et al., in preparation).

whether shocked fast stellar wind, collimated outflows or both are responsible for the X-ray emission from PNe.

The Eskimo Nebula (NGC 2392) offers an excellent opportunity to assess the effects of collimated outflows in a PN. The Eskimo is a double-shell PN: its bright elliptical inner shell has two blister-like protrusions on the south rim, and its round outer shell contains a set of complex low-ionization features (O'Dell et al., 2002). In addition, the Eskimo has a fast collimated outflow, detected in high-dispersion spectra of optical nebular lines; the outflow, with line-of-sight expansion velocities approaching 200 km s^{-1} , is dynamically interacting with nebular material (Giesekeing, Becker, & Solf, 1985; O'Dell & Ball, 1985; O'Dell, Weiner, & Chu, 1990, Maestro et al., in preparation). We have obtained *XMM-Newton* observations of the Eskimo and here we report the detection of diffuse X-ray emission from this nebula.

2. Observations

The Eskimo Nebula was observed with the *XMM-Newton* Observatory in Revolution 790 on 2004 April 2 using the EPIC/MOS1, EPIC/MOS2, and EPIC/pn CCD cameras. The two EPIC/MOS cameras were operated in the Full-Frame Mode for a total exposure time of 17.5 ks, while the EPIC/pn camera was operated in the Extended Full-Frame Mode for a total exposure time of 12.5 ks. For all observations, the Medium filter was used. The *XMM-Newton* pipeline products were processed using the *XMM-Newton* Science Analysis Software (SAS version 6.0.0) and the calibration files from the Calibration Access Layer available on 2004 June 10.

The event files were screened to eliminate events due to charged particles or associated with periods of high background. For the EPIC/MOS observations, only events with CCD patterns 0–12 (similar to *ASCA* grades 0–4) were selected; for the EPIC/pn observation, only events with CCD pattern 0 (single pixel events) were selected. Time intervals with high background (i.e. count rates $\geq 0.3 \text{ cnts s}^{-1}$ for

the EPIC/MOS or $\geq 1.4 \text{ cnts s}^{-1}$ for the EPIC/pn in the background-dominated 10–12 keV energy range) were discarded. The resulting exposure times are 17.3 ks, 17.1 ks, and 11.6 ks for the EPIC/MOS1, EPIC/MOS2, and EPIC/pn observations, respectively.

3. Results

The *XMM-Newton* EPIC/MOS1, EPIC/MOS2, and EPIC/pn observations of the Eskimo detect within the nebula a total of 180 ± 15 , 175 ± 15 , and 620 ± 30 cnts, respectively. In order to construct an X-ray image of the highest signal-to-noise ratio, we merged together the event files of the three EPIC observations and extracted raw EPIC images in the 0.2–2.0, 0.2–0.65, and 0.65–2.0 keV bands with a pixel size of $1''.5$ (Fig. 1a, 1c and 1d). The raw EPIC image in the 0.2–2.0 keV band is then adaptively smoothed using Gaussian profiles with FWHM ranging from $4''$ to $6''$. The contour map of this smoothed image is overplotted on a *Hubble Space Telescope* (*HST*) Wide Field Planetary Camera 2 (WFPC2) $H\alpha$ image (Fig. 1b). The alignment of X-ray and optical images is fine-tuned using HD 59087, a star $\sim 100''$ north of the Eskimo, which is detected both in the *XMM-Newton* EPIC and *HST* WFPC2 images.

The X-ray emission from the Eskimo is clearly extended. Its distribution is elongated along $\text{PA} \sim 25^\circ$ (Fig. 1a), and the 25% contour of the smoothed EPIC image follows closely the outline of the inner shell in the *HST* $H\alpha$ image (Fig. 1b). The image in the 0.2–0.65 keV band shows a similar spatial distribution, but in the 0.65–2.0 keV band the emission is elongated along $\text{PA} \sim 70^\circ$, i.e., roughly aligned with the fast bipolar outflow detected at PAs of 50° – 80° and 230° – 260° , as illustrated in Fig. 1d (Giesekeing, Becker, & Solf, 1985, Maestro et al., in preparation). These comparisons suggest that the diffuse X-ray emission from the Eskimo is mostly confined within its inner shell, but some of the harder X-ray emission in the 0.65–2.0 keV band may be produced by the interaction of the fast bipolar outflow with nebular material.

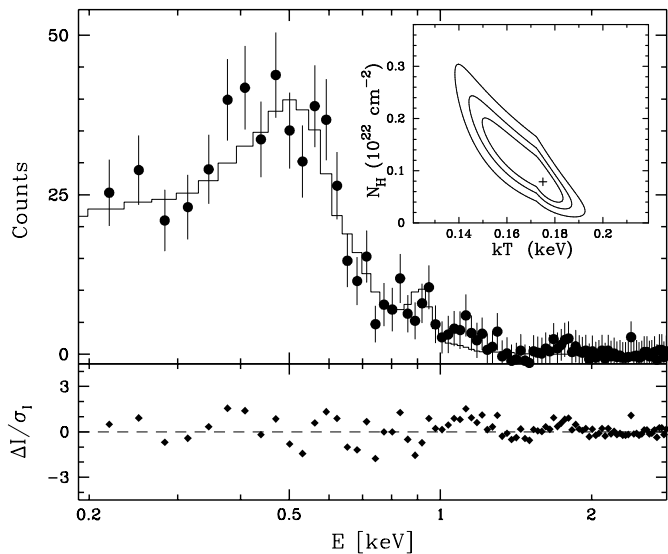


Fig. 2. (top) *XMM-Newton* EPIC/pn background-subtracted spectrum of the Eskimo overplotted with the best-fit MEKAL model. For plotting purposes, both the spectrum and model are binned in 30 eV wide energy bins. (inset) χ^2 grid plot as a function of kT and N_{H} of the spectral fit to the EPIC/pn spectrum. The contours represent 68%, 90%, and 99% confidence levels. (bottom) Relative residuals of the best-fit model to the EPIC/pn spectrum.

To analyze the properties of the diffuse X-ray emission from the Eskimo, we extracted a spectrum from the EPIC/pn event file using a circular source aperture of $20''$ radius, large enough to include all X-ray emission from the nebula. The background level was assessed from an annular region exterior to the source aperture and 9 times larger in area. The background-subtracted EPIC/pn spectrum of the Eskimo is shown in Fig. 2. This spectrum shows a broad peak between 0.4 and 0.6 keV, a plateau below 0.4 keV, and a sharp decline above 0.6 keV. Low-intensity emission peaks are discernible at ~ 0.9 keV, ~ 1.1 keV, and ~ 1.8 keV. The overall spectral shape indicates thermal plasma emission, and the peaks correspond to the He-like triplets of N VI at ~ 0.43 keV, O VII at ~ 0.57 keV, Ne IX at ~ 0.92 keV, Na X at ~ 1.13 keV, and Si XIII at ~ 1.86 keV. We have also extracted EPIC/MOS spectra; they show similar spectral features at lower signal-to-noise ratios, so we will concentrate only on the EPIC/pn spectrum in the analysis below.

The observed spectrum can be modeled to determine the physical conditions of the X-ray-emitting gas and the amount of foreground absorption. We have adopted the MEKAL optically-thin plasma emission model (Kaastra & Mewe, 1993; Liedhal, Osterheld, & Goldstein, 1995) and nebular abundances, although we note that these may differ from those of the X-ray-emitting gas (e.g., Maness et al., 2003). The abundances of He, C, N, O, Ne, Ar, and S relative to hydrogen by number, as determined from optical and UV spectra of the Eskimo, are 0.076, 2.2×10^{-4} , 1.1×10^{-4} , 2.8×10^{-4} , 6.4×10^{-5} , 1.4×10^{-6} , and 4.3×10^{-6} , respectively (Barker, 1991; Henry, Kwitter & Bates, 2000). For elements that do not have available nebular abundances, we

adopt solar abundances (Grevesse & Sauval, 1998). We have also assumed solar abundances for the foreground interstellar absorption, and adopted absorption cross-sections from Balucinska-Church & McCammon (1992).

The spectral fit is carried out by folding the absorbed MEKAL model spectrum through the EPIC/pn response matrix, and comparing the modeled spectrum to the observed EPIC/pn spectra in the 0.2–2.5 keV energy range using the χ^2 statistics. The best-fit model with nebular abundances has a large reduced χ^2 , ~ 2.5 , with excessive positive residuals at ~ 0.4 keV and ~ 0.9 keV and negative residuals at ~ 0.6 keV. These energies are coincident with the N VI, Ne IX, and O VII lines, respectively; thus the residuals suggest that the N/O and Ne/O abundance ratios are higher than those of the adopted nebular values. We have therefore made spectral fits that allowed the abundances of N and Ne to vary, and subsequently the reduced χ^2 is improved to ~ 1.5 .

The best-fit model, overplotted on the EPIC/pn spectrum in Fig. 2, has a plasma temperature of $T = (2.0_{-0.3}^{+0.1}) \times 10^6$ K (or $kT = 0.175_{-0.03}^{+0.01}$ keV), an absorption column density $N_{\text{H}} = (8_{-5}^{+12}) \times 10^{20}$ cm $^{-2}$, and a volume emission measure of $(1.2 \pm 0.3) \times 10^{54} (d/1150 \text{ pc})^2$ cm $^{-3}$, where d is the distance in parsecs and has been reported to be 1150 pc (Perryman et al., 1997). The quality of the spectral fits is illustrated by the plot of the reduced χ^2 of the fits as a function of kT and N_{H} shown in the inset of Fig. 2. Adopting a typical gas-to-dust ratio (Bohlin, Savage, & Drake, 1978), the best-fit absorption column density corresponds to a logarithmic extinction at the H β line of $c_{\text{H}\beta} = 0.2_{-0.1}^{+0.3}$, in agreement with that determined from the Balmer decrement (Barker, 1991). The N and Ne abundances are enhanced with respect to the nebular abundances by 3.5 ± 1.2 and 3.0 ± 1.0 , respectively, thus resulting in N/O ~ 1.4 and Ne/O ~ 0.7 . The residuals of the best-fit model may also indicate enhanced Na and Si abundances, but the number of counts is too small to warrant spectral fits allowing these abundances to vary.

The observed (absorbed) X-ray flux in the 0.2–2.5 keV energy range is $(6 \pm 1) \times 10^{-14}$ ergs cm $^{-2}$ s $^{-1}$, and the intrinsic (unabsorbed) X-ray flux is $(1.6 \pm 0.6) \times 10^{-13}$ ergs cm $^{-2}$ s $^{-1}$. The X-ray luminosity in the same energy range is $L_{\text{X}} = (2.6 \pm 1.0) \times 10^{31} (d/1150 \text{ pc})^2$ ergs s $^{-1}$.

4. Discussion

The sharp rim of the Eskimo’s inner shell suggests compression by supersonic shocks. Indeed, the inner shell of the Eskimo, expanding at ~ 90 km s $^{-1}$ into the much slower outer shell, has an expansion velocity notably high among PNe (O’Dell & Ball, 1985). To assess whether the hot gas in the central cavity is responsible for driving such a fast expansion, we derive the thermal pressure of the X-ray-emitting gas and compare it to those of the surrounding nebular shells. Assuming a prolate ellipsoidal central cavity, the volume occupied by the X-ray-emitting gas is $\sim 1.1 \times 10^{51} (d/1150 \text{ pc})^3 (\epsilon/0.5)$ cm 3 , where ϵ is the filling factor and may be ~ 0.5 . From this volume and the aforementioned volume emission measure, we derive an rms electron density of $n_{\text{e}} \sim 35 (d/1150 \text{ pc})^{-1/2} (\epsilon/0.5)^{-1/2}$ cm $^{-3}$. This rms electron density and the plasma temperature of $2.0 \times$

10^6 K imply that the thermal pressure of the X-ray-emitting gas, $P_{\text{th}} \sim 1.9 \times n_e kT$, is $\sim 2 \times 10^{-8} (d/1150\text{pc})^{-1/2} (\epsilon/0.5)^{-1/2}$ dynes cm^{-2} . The inner and outer shells of the Eskimo have densities of 2500 and 900 cm^{-3} , respectively, and a temperature of 14,500 K (Barker, 1991). The thermal pressure of the inner and outer shells are $\sim 1 \times 10^{-8}$ and $\sim 3 \times 10^{-9}$ dynes cm^{-2} , respectively. The X-ray-emitting gas has slightly higher thermal pressure than the inner shell, and much higher than the outer shell, thus the thermal pressure of the hot gas in the Eskimo's central cavity drives the expansion of its inner shell into the outer shell.

The temperature of the X-ray-emitting gas in the Eskimo, 2.0×10^6 K, is similar to that found in other elliptical PNe; however, the terminal velocity of the Eskimo's fast wind is low, only ~ 400 km s^{-1} (Pauldrach, Hoffmann, & Méndez, 2003). For an adiabatic shock, the expected temperature of the shocked wind would be $\sim 1.9 \times 10^6$ K for such a velocity, barely reaching the temperature indicated by the X-ray spectrum, in sharp contrast to other PNe whose shocked stellar winds are 10–100 times hotter than the hot gas detected (e.g., Chu et al., 2001; Kastner et al., 2000). If the hot gas in the Eskimo indeed originates from the shocked fast stellar wind, the low expected post-shock temperature implies that no significant mixing of nebular material has taken place. The mass of the hot gas, $\sim 3 \times 10^{-5} (d/1150\text{pc})^{5/2} (\epsilon/0.5)^{1/2} M_{\odot}$, can be supplied by the fast stellar wind in ~ 1800 yr at a constant mass loss rate of $1.8 \times 10^{-8} M_{\odot} \text{ yr}^{-1}$ (Pauldrach, Hoffmann, & Méndez, 2003).

If the X-ray emission from the Eskimo does not originate from a shocked fast stellar wind, then there are two other possibilities. First, the X-ray emission can be partially attributed to the central star as in the case of NGC 6543 or to a late-type binary companion as in the case of NGC 7293 (Guerrero et al., 2001). The angular resolution of *XMM-Newton*, however, is insufficient to resolve a point source from the diffuse emission from the Eskimo. Second, the diffuse X-ray emission can be produced by the dynamical interaction of the fast bipolar outflow with the inner shell. This collision will produce shock-excited gas along the direction of the outflow which is detected as the harder X-ray emission in the 0.65–2.0 keV band, and also as shock-excited [Fe II] 1.26 and 1.64 μm line emissions (Hollenbach & McKee, 1989; Hora, Latter, & Deutsch, 1999). Similar situation is observed in BD+30°3639, whose diffuse X-ray emission shows an asymmetric spatial distribution in hard energies and reveals spectral evidence of enhanced Ne/O abundance ratio (Kastner et al., 2002). As suggested for BD+30°3639 (Soker & Kastner, 2003), the hottest gas in the Eskimo may have been produced by a fast, ~ 500 km s^{-1} , collimated post-AGB wind that is no longer present. Alternatively, the observed 200 km s^{-1} outflow may have a large inclination with respect to the line-of-sight, so that its real expansion velocity is large enough to power the hottest gas in the Eskimo.

Our *XMM-Newton* observations of the Eskimo Nebula have detected diffuse X-ray emission from hot gas within its central cavity. The high thermal pressure of this hot gas is responsible for the high expansion velocity of its innermost shell. The origin of this hot gas, however, is uncertain, and may consist of several components: shocked fast stellar wind, shocks associated with the fast bipolar outflow, and emission from its central star or a binary companion. X-ray observations at the high-

est spatial resolution afforded by *Chandra* are needed to determine accurately the origin of X-ray emission from the Eskimo Nebula, a very interesting and complex PN.

Acknowledgements. M.A.G. is grateful to the VILSPA staff for his help and hospitality during the 4th SAS Workshop held in VILSPA on June 8–12 2004. M.A.G. also acknowledges support from the grant AYA 2002-00376 of the Spanish MCyT (cofunded by FEDER funds). Y.-H.C. acknowledges support from the NASA grant NNG04GE63G.

References

- Balucinska-Church, M., & McCammon, D. 1992, *ApJ*, 400, 699
- Barker, T. 1991, *ApJ*, 371, 217
- Bohlin, R. C., Savage, B. D., & Drake, J. F. 1978, *ApJ*, 224, 132
- Bobrowsky, M. et al. 1995 *ApJ*, 446, L89
- Cerruti-Sola, M. & Perinotto, M. 1985, *ApJ*, 291, 237
- Chu, Y.-H., Chang, T. H., & Conway, G. M. 1997, *ApJ*, 482, 891
- Chu, Y.-H., Guerrero, M. A., Gruendl, R. A., Williams, R. M., & Kaler, J. B. 2001, *ApJ*, 553, L69
- Giesekeing, F., Becker, I., & Solf, J. 1985, *ApJ*, 295, L17
- Grevesse, N., & Sauval, A. J. 1998, *Space Sci. Rev.*, 85, 161
- Guerrero, M. A., Chu, Y.-H., & Gruendl, R. A. 2000, *ApJS*, 129, 295
- Guerrero, M. A., Chu, Y.-H., Gruendl, R. A., Williams, R. M., & Kaler, J. B. 2001, *ApJ*, 553, L55
- Guerrero, M. A., Gruendl, R. A., & Chu, Y.-H. 2002, *A&A*, 387, L1
- Henry, R. B. C., Kwitter, K. B., & Bates, J. A. 2000, *ApJ*, 531, 928
- Hollenbach, D. & McKee, C. F. 1989, *ApJ*, 342, 306
- Hora, J. L., Latter, W. B., & Deutsch, L. K. 1999, *ApJS*, 124, 195
- Kaastra, J. S., & Mewe, R. 1993, *Legacy*, 3, 16, HEASARC, NASA
- Kastner, J. H., Balick, B., Blackman, E. G., Frank, A., Soker, N., Vrřilek, S. D., & Li, J. 2003, *ApJ*, 591, L37
- Kastner, J. H., Li, J., Vrřilek, S. D., Gatley, I., Merrill, K. M., & Soker, N. 2002, *ApJ*, 581, 1225
- Kastner, J. H., Soker, N., Vrřilek, S. D., & Dgani, R. 2000, *ApJ*, 545, L57
- Kastner, J. H., Vrřilek, S. D., & Soker, N. 2001, *ApJ*, 550, L189
- Kwok, S., Purton, C. R., & Fitzgerald, P. M. 1978, *ApJ*, 219, L125
- Liedahl, D. A., Osterheld, A. L., & Goldstein, W. H. 1995, *ApJ*, 438, L115
- Maness, H. L., Vrřilek, S. D., Kastner, J. H., & Soker, N. 2003, *ApJ*, 589, 439
- O'Connor, J. A., Redman, M. P., Holloway, A. J., Bryce, M., López, J. A., & Meaburn, J. 2000, *ApJ*, 531, 336
- O'Dell, C. R., Balick, B., Hajian, A. R., Henney, W. J., & Burkert, A. 2002, *AJ*, 123, 3329
- O'Dell, C. R. & Ball, M. E. 1985, *ApJ*, 289, 526
- O'Dell, C. R., Weiner, L. D., & Chu, Y.-H. 1990, *ApJ*, 362, 226
- Pauldrach, A. W. A., Hoffmann, T. L., & Méndez, R. H. 2003, *IAU Symposium*, 209, 177

- Perryman, M. A. C. et al., 1997, *A&A*, 323, L49
- Riera, A., García-Lario, P., Manchado, A., Pottasch, S. R., & Raga, A. C. 1995, *A&A*, 302, 137
- Sahai, R., Kastner, J. H., Frank, A., Morris, M., & Blackman, E. G. 2003, *ApJ*, 599, L87
- Soker, N. & Kastner, J. H. 2003, *ApJ*, 583, 368
- Weaver, R., McCray, R., Castor, J., Shapiro, P., & Moore, R. 1977, *ApJ*, 218, 377